SAND2017-13049R

SAND20XX-XXXXR
LDRD PROJECT NUMBER: 180897
LDRD PROJECT TITLE: Dual-Particle Imaging System with Neutron Spectroscopy for Safeguard Applications
PROJECT TEAM MEMBERS: Michael Hamel and Tom Weber

ABSTRACT:

A dual-particle imager (DPI) has been designed that is capable of detecting gamma-ray and neutron signatures from shielded SNM. The system combines liquid organic and NaI(Tl) scintillators to form a combined Compton and neutron scatter camera. Effective image reconstruction of detected particles is a crucial component for maximizing the performance of the system; however, a key deficiency exists in the widely used iterative list-mode maximum-likelihood estimation-maximization (MLEM) image reconstruction technique. For MLEM a stopping condition is required to achieve a good quality solution but these conditions fail to achieve maximum image quality. Stochastic origin ensembles (SOE) imaging is a good candidate to address this problem as it uses Markov chain Monte Carlo to reach a stochastic steady-state solution. The application of SOE to the DPI is presented in this work.

SOE was originally applied in medical imaging applications with no mechanism to isolate spectral information based on location. This project extends the SOE algorithm to produce spatially dependent spectra and presents experimental result showing that the technique was effective for isolating a 4.1-kg mass of weapons grade plutonium (WGPu) when other neutron and gamma-ray sources were present.

This work also demonstrates the DPI as an effective tool for localizing and characterizing highly enriched uranium (HEU). A series of experiments were performed with the DPI using a deuterium-tritium (DT) neutron generator to interrogate a 13.7-kg sphere of HEU. The neutrons and gamma rays produced from induced fission were successfully discriminated from the interrogating particles to localize the HEU.

Sandia National Laboratories is a multimission laboratory managed and operated by National Technology and Engineering Solutions of Sandia LLC, a wholly owned subsidiary of Honeywell International Inc. for the U.S. Department of Energy's National Nuclear Security Administration under contract DE-NA0003525.

INTRODUCTION:

Nuclear proliferation presents a great challenge to society today and agreements such as arms-control treaties and the Non Proliferation Treaty (NPT) seek to stop the spread of nuclear weapons and technologies and eliminate existing weapons. These agreements require means of verification to ensure compliance of all parties. Radiation detection has played a role in arms-control treaties such as the Intermediate Nuclear Forces (INF) Treaty, the Strategic Arms Reduction Treaty (START) and the New Strategic Arms Reduction Treaty (New START). However, in these agreements, the radiation detection equipment (RDE) consisted solely of a simple He-3 neutron counter. For the INF Treaty, the detector measured count rates at different locations near a missile, a crude form of imaging, and compared that profile with a trusted template. For START and New START, the same detector was used but only to verify that an item declared as non-nuclear was in fact non-nuclear. With new potential future treaties that seek to more vigorously verify a warhead, technical advances are needed in RDE that can go beyond verification of simple count rates.

One candidate for this task is radiation imaging. This technique offers several advantages over simple counting. For example, an imager can dwell on a treaty accountable item that contains several declared warheads and create an image showing the true number of warheads the item contains. High resolution imaging can even show the shape of the fissile material. Most radiation imaging systems have sensitivity to only one type of particle emitted from special nuclear material (SNM), gamma rays or neutrons. An imager capable of reconstructing both neutron and gamma-ray images would provide more complete information and be more robust to shielding and spoofing scenarios.

This project examined the application of the Dual-Particle Imager (DPI), designed at the University of Michigan, to SNM detection [1,2]. Typical SNM sources such as weapons-grade plutonium (WGPu) and highly enriched uranium (HEU) emit both neutrons and gamma rays through spontaneous fission and radioactive decay. The DPI is an excellent instrument for SNM detection because it has sensitivity to both neutrons and gamma rays as well as spectroscopic capabilities for both particle types. The system uses organic liquid and NaI(Tl) scintillators. The organic liquid scintillators can detect both neutrons and gamma rays and have excellent timing properties and particle discrimination capability. The NaI(Tl) scintillators provide a high-efficiency low cost method for detecting gamma rays.

The first aspect of this work included application of the Stochastic Origin Ensembles (SOE) method, which was originally applied to medical imaging applications, for both neutrons and gamma rays [3]. SOE relies on a Markov chain Monte Carlo process. Using this method addresses a shortcoming with the widely used maximum-likelihood estimation-maximization (MLEM) technique. Both techniques are iterative methods; however, the steady-state solutions of both image reconstruction methods provide different image quality. For SOE, the steady-state solution is the optimum solution but for MLEM, the steady state solution will have worse qualities than solutions at previous iterations. Determining the proper stopping condition to achieve optimum image quality is still an open area of research with best efforts only providing up to 80% of the

Sandia National Laboratories is a multimission laboratory managed and operated by National Technology and Engineering Solutions of Sandia LLC, a wholly owned subsidiary of Honeywell International Inc. for the U.S. Department of Energy's National Nuclear Security Administration under contract DE-NA0003525.

best solution [4]. This work also modified the SOE method to include spatial isolation of measured energy spectra, a useful technique when more than one source is present. The capabilities of the DPI were also demonstrated in two measurement campaigns at the Device Assembly Facility (DAF) located within the Nation Nuclear Security Site in Nevada. The first campaign focused on detection of WGPu and the second featured active interrogation to detect HEU enriched to 93% ^{235}U.

DETAILED DESCRIPTION OF EXPERIMENT/METHOD:

THE DUAL-PARTICLE IMAGER

The DPI, shown in Fig. 1, is a combined neutron and Compton scatter camera built in a two-plane design. The front-plane is composed of a 4×4 array of EJ-309 liquid organic scintillators and acts as a scatter plane for both neutrons and gamma-rays. The organic scintillators have excellent pulse shape discrimination capabilities allowing accurate identification of whether a detected event was a neutron or gamma-ray. The back-plane is a 4×4 array of organic liquid and NaI(Tl) scintillators interspersed in a checkboard pattern. The organic liquid scintillators act as a back-plane for the neutron scatter camera portion of the DPI while the NaI(Tl) scintillators act as the absorption plane for the Compton camera portion of the DPI. The front plane liquid scintillators are each 5.1 cm thick with a 7.6-cm diameter. The back plane detectors (both organic liquid and NaI(Tl) scintillators) each have a 7.6-cm thickness and 7.6-cm diameter. The front plane has a center-to-center detector spacing of 15 cm and the back-plane a center-to-center detector spacing of 25 cm.

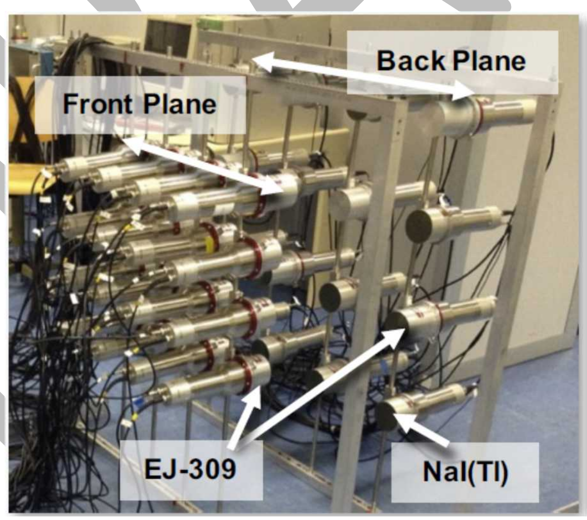

Figure 1. Photo of the Dual-Particle Imager

To detect a neutron that can be used for image reconstruction, a detection of the same neutron in a front-plane organic liquid scintillator followed by a detection in a back-plane organic liquid scintillator is required. Double-scatter events in the system creating imageable events are referred to as correlated counts. Ideally, the neutron will have undergone a single elastic scatter interaction on hydrogen in both detectors. The energy of the incident neutron, $\mathbf{E_{0,n}}$, is calculated by

$$E_{0,n} = E_{1,n} + E_{TOF},$$

where $\mathbf{E_{1,n}}$, is the energy deposited in the front-plane detector and $\mathbf{E_{TOF}}$ is the remaining energy of the neutron after the first scatter calculated by measuring the time-of-flight between detections in both detectors. The incident energy $\mathbf{E_{0,n}}$ and the energy deposition in the first detector $\mathbf{E_{1,n}}$ are used in the equation

$$\theta_n = \cos^{-1}\sqrt{\frac{E_{1,n}}{E_{0,n}}},$$

to calculate $\boldsymbol{\theta_n}$, which represents the opening angle of a cone relative to the axis between both detectors. The surface of the cone contains the set of possible origins for the detected neutron. Fig. 2 shows a diagram of a detected neutron and the cone of possible source locations.

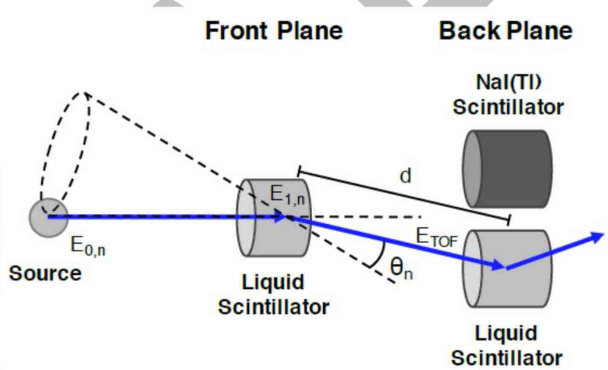

Figure 2. Schematic of a neutron event

Gamma-ray detection in the DPI is analogous to the neutron detection in that the energy of the incident gamma ray is calculated and a cone of possible source origins is constructed. The incident gamma-ray energy $\mathbf{E_{0,\gamma}}$, is calculated using

$$E_{0,\gamma} = E_{1,\gamma} + E_{2,\gamma},$$

where $\mathbf{E_{1,\gamma}}$, is the energy deposited in a front-plane organic liquid scintillator and $\mathbf{E_{2,\gamma}}$ is the energy deposited in a back-plane NaI(Tl) scintillator. The opening angle of the cone $\boldsymbol{\theta_\gamma}$, is then calculated using the equation

$$\theta_\gamma = \cos^{-1}\left[1 - \frac{m_e c^2 E_{1,\gamma}}{E_{2,\gamma}(E_{1,\gamma}+E_{2,\gamma})}\right].$$

Fig. 3 shows the cone of possible source locations that is generated by a gamma-ray detected in the system. As for a neutron event, an ideal gamma-ray event is a single scatter in a front plane organic liquid scintillator followed by a full energy absorption in a back-plane NaI(Tl).

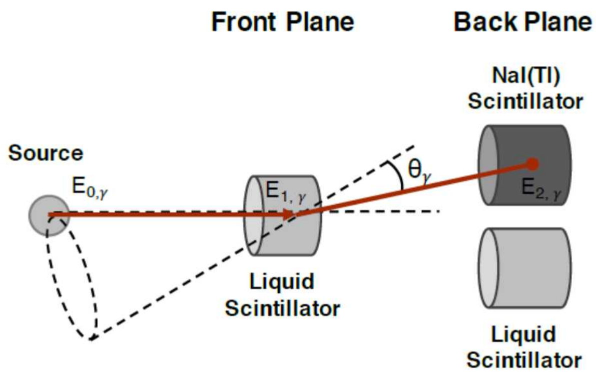

Figure 3. Schematic of a gamma-ray event

Obtaining the incident energy of both neutrons and gamma rays provides spectroscopic capabilities and the cones of possible source locations allow for image reconstruction. A superposition of measured cones produces what is known as a backprojection image.

STOCHASTIC ORIGIN ENSEMBLES ALGORITHM

SOE image reconstruction is based on the backprojection images, but improves the resolution by limiting the set of possible source locations to a single origin instead of an entire cone. The SOE method, which uses the Metropolis Hastings algorithm is implemented as follows separately for neutrons and gamma rays:

1. For each event, a single possible source position is sampled on the intersection of the cone, representing possible source locations, and a sphere surrounding the system. This sampled location is referred to as an origin. The collection of origins from each cone creates the starting image state.
2. A new, potential image state is created by randomly selecting a single origin, and re-sampling its location on the cone-sphere intersection. The number of origins located at the new pixel, in the potential image state is compared to the number of origins located at the old pixel, in the current image state.
3. The new location of the origin will be accepted or rejected based on an acceptance probability, **A**, defined as

$$A(I_s \rightarrow I_{s+1}) = \min\left(1, \frac{N_{p\prime,s+1}}{N_{p,s}}\right),$$

where $\mathbf{I_s}$ is the current image state, $\mathbf{I_{s+1}}$ is the proposed image state, $\mathbf{N_{p',s+1}}$ is the number of origins in pixel **p'** in the proposed image state, and $\mathbf{N_{p,s}}$ is the number of origins in pixel **p** in the current image state.

4. The repetition of steps 2 and 3 for each origin defines a single iteration of the algorithm. A number of iterations are performed. A running average of all image states in the Markov chain creates the reconstructed image. Once the image reaches a quasi-steady state iterations are stopped.

To include spatial isolation of spectra, image states were dived into energy bins. Each origin has an associated energy so origins were sampled and re-sampled in images according to their respective energy. When determining the acceptance probability, **A**, in step 3, the images were summed. The final solution provides the necessary information to create an energy spectrum for each pixel.

PASSIVE WGPU EXPERIMENTS

To demonstrate gamma-ray and neutron spectrum isolation for Category-I SNM, the DPI was used for passive detection experiments at the DAF. The DAF provided a 4.1-kg disk of WGPu that measured 10.64 cm in diameter and had a thickness of 2.52 cm. The WGPu was measured in the presence of two other neutron and gamma-ray emitting sources, ^{252}Cf and AmBe. The WGPu had the coordinates (90°, 85°) and had an emission of approximately 5.2×10^5 neutrons per second. The coordinate system was arranged such that the coordinate (90°, 90°) is centered directly in front of the DPI. The ^{252}Cf was located at (90°, 109°) and had an emission rate of approximately 3×10^5 neutrons per second. The AmBe was placed at (141°, 85°) and emitted approximately 1×10^6 neutrons per second. The WGPu, ^{252}Cf, and AmBe sources were located 201 cm, 212 cm, and 207 cm from the DPI respectively and were measured for 850 min. Fig. 4 shows the sources in relation to the DPI. A 1.3 cm lead shadow-shield was placed 30 cm in front of the WGPu to help reduce the large flux of low energy gamma-rays – particularly the 0.0595-MeV emission from built up ^{241}Am, which has a specific activity of 4.54×10^{10} gamma-rays per second per gram. The AmBe was also shielded with about 10 cm of lead to accommodate another detection system that was measuring concurrently with the DPI.

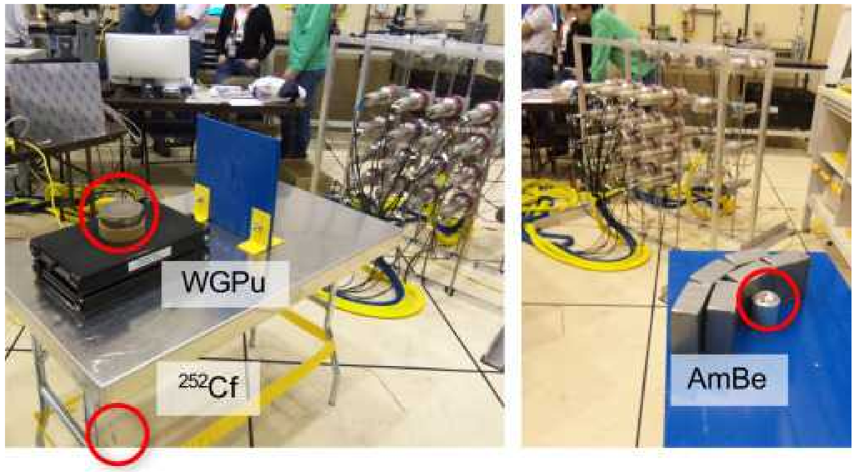

Figure 4. Experimental setup for passive WGPu detection

ACTIVE HEU EXPERIMENTS

HEU does not have a neutron emission significant enough for passive detection. The gamma-ray emissions are also low energy and therefore easily shielded. A 13.7-kg sample of HEU was provided by the DAF and a deuterium-tritium (DT) neutron generator, which produced 14.1-MeV neutrons with an output of 7×10^7 neutrons per second isotropically, was used to induce fission reactions in the HEU. The DT neutron generator was placed on an aluminum table at a distance of 158 cm from the center of the DPI. The target in the DT neutron generator had angular coordinates of (100°, 86°). The sample being interrogated was placed on the table with the sample center at a distance of 155 cm and angular coordinates of (90°, 86°). Several configurations with different moderation or shielding were measured. A bare configuration was measured for 59 minutes. A case with no item present was measured for seven minutes. Fig. 5 shows a photograph of the experimental setup for the bare HEU configuration. A high-density polyethylene (HDPE) moderator was used, which was a 3.81-cm thick shell that left a 2-cm gap between the inside of the shell and the HEU when surrounding it. A 22-minute measurement was taken with the HDPE moderator.

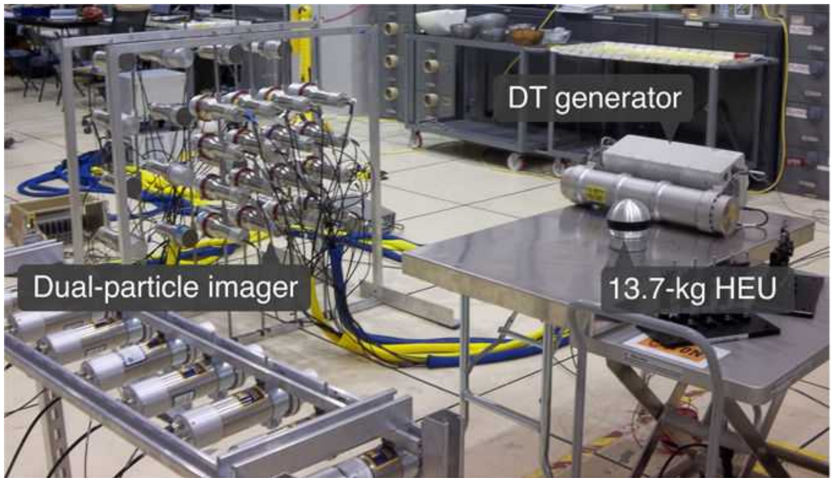

Figure 5. Experimental setup for active interrogation of HEU

RESULTS:

PASSIVE WGPU EXPERIMENTS

The reconstructed neutron image shows three hot-spots in Fig. 6. To generate this reconstruction, 1×10^5 iterations of the SOE algorithm were used with 0.10-MeV energy bin widths and a total of 161,189 neutron events. Each cone was projected onto a sphere with a radius of 200 cm.

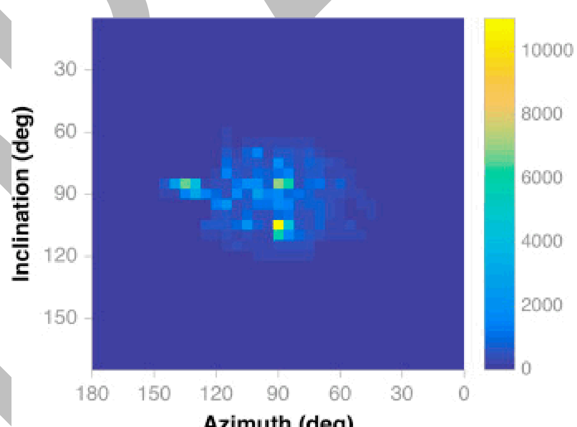

Figure 6. Neutron image for measurement of ^{252}Cf, AmBe, and WGPu

The isolated neutron spectra, shown in Fig. 7(a), for each hot-spot for the WGPu, ^{252}Cf, and AmBe were generated from 3×3-pixel regions centered at (90°, 85°), (90°, 105°), and (135°, 85°) respectively. The spectra were normalized for comparison and are shown in Fig. 7(b). The shapes for the WGPu and ^{252}Cf hot-spots are similar as expected, with average energies of 3.23 MeV and 3.20 MeV respectively, since both sources emit neutrons in a Watt distribution. However, the

AmBe spectrum has a different shape with a larger fraction of neutrons being emitted at higher energies and an average energy of 3.85 MeV.

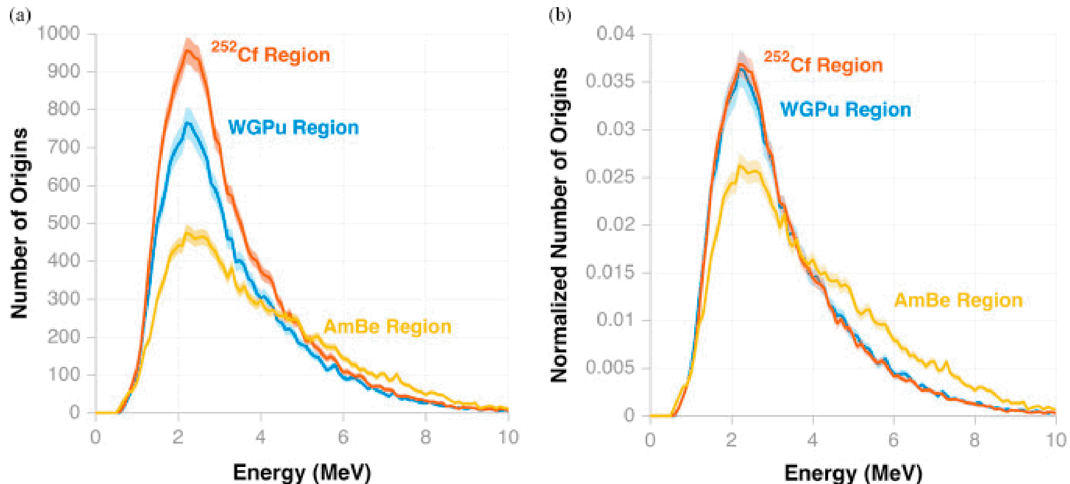

Figure 7. Isolated neutron spectra (a) for measurement of ^{252}Cf, AmBe, and WGPu and the normalized spectra (b)

The reconstructed gamma-ray image, in Fig. 8, showed only two hot-spots, which located the WGPu and the ^{252}Cf. A hot-spot is not seen for the AmBe because of the 10-cm lead shield placed in between it and the DPI. A total of 1×10^5 iterations were used in the reconstruction.

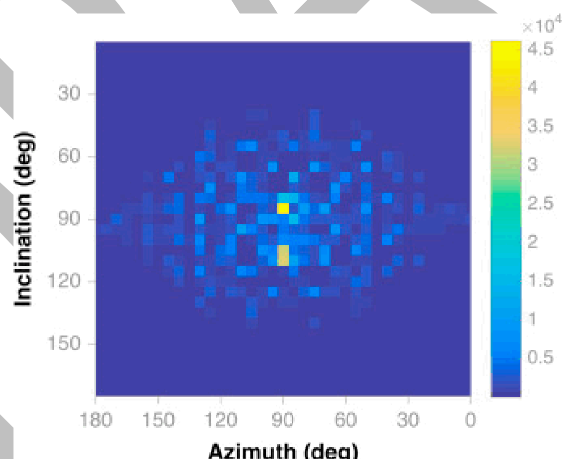

Figure 8. Gamma-ray image for measurement of ^{252}Cf, AmBe, and WGPu

The isolated spectra were taken from 3×3-pixel regions centered at (90°, 85°) and (90°, 110°) and are shown in Fig. 9(a). A comparison of the normalized spectra is shown in Fig. 9(b). The spectrum isolated from the WGPu showed a peak at 0.64 MeV that is less prominent in the isolated spectrum from ^{252}Cf. The peak in the WGPu spectrum is a result of decay gamma-rays from ^{239}Pu and ^{241}Am, which were both isotopes present in the sample. The WGPu contained approximately 205 g of ^{240}Pu which has a specific activity of 1.05×10^3 for the 0.642 keV gamma-ray. The peak at 0.62

MeV in the ^{252}Cf spectrum was due to fission products that built up in the source and some contamination from origins that were actually produced from the WGPu. The ^{252}Cf had an approximate age of 10 years. A feature was also seen in the ^{252}Cf spectrum at about 0.48 MeV. This feature can be attributed to photon production from the (n,α) reaction on ^{10}B, which composed part of the optical windows in the EJ-309 liquid scintillators. This feature is not seen in the WGPu spectrum because the source-to-background ratio is larger so it is washed out and other gamma ray energies are present in this region.

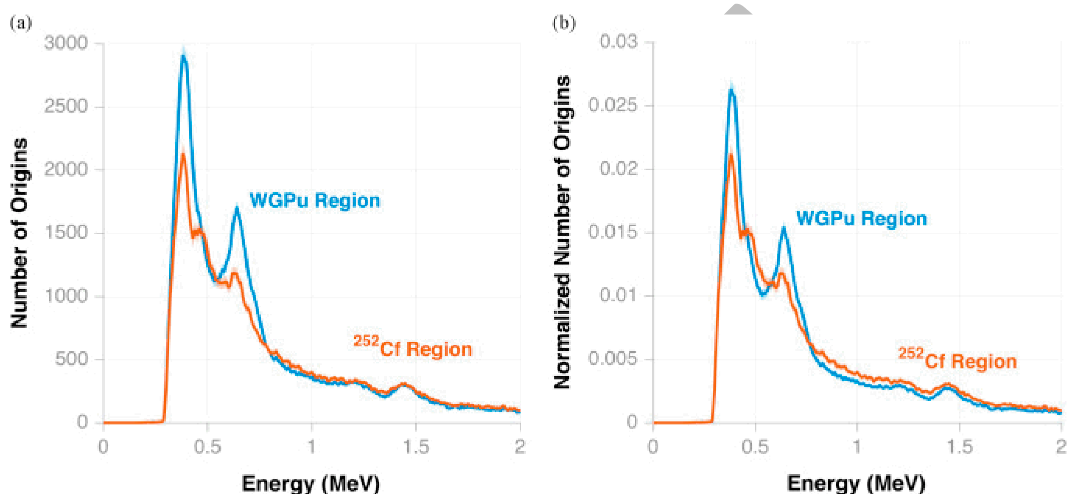

Figure 9. Isolated gamma-ray spectra (a) for measurement of ^{252}Cf, AmBe, and WGPu and the normalized spectra (b)

ACTIVE HEU EXPERIMENTS

The reconstructed images for the case with no item, the bare HEU, and HDPE-moderated HEU are compared in Fig. 10. The neutron and gamma-ray images for the bare HEU case, Fig. 10(c) and (d) respectively, were scaled for maximum contrast between the maximum and minimum pixel value. For the case with no item, the images were displayed using the same scale as when the bare HEU sphere was used as the target. This scale helps to highlight the increased correlated count rates from the HEU target. In all images, a red and green box are overlaid to show the positions of the DT neutron generator and target, respectively. The scale values in all cases are in units of correlated counts per second.

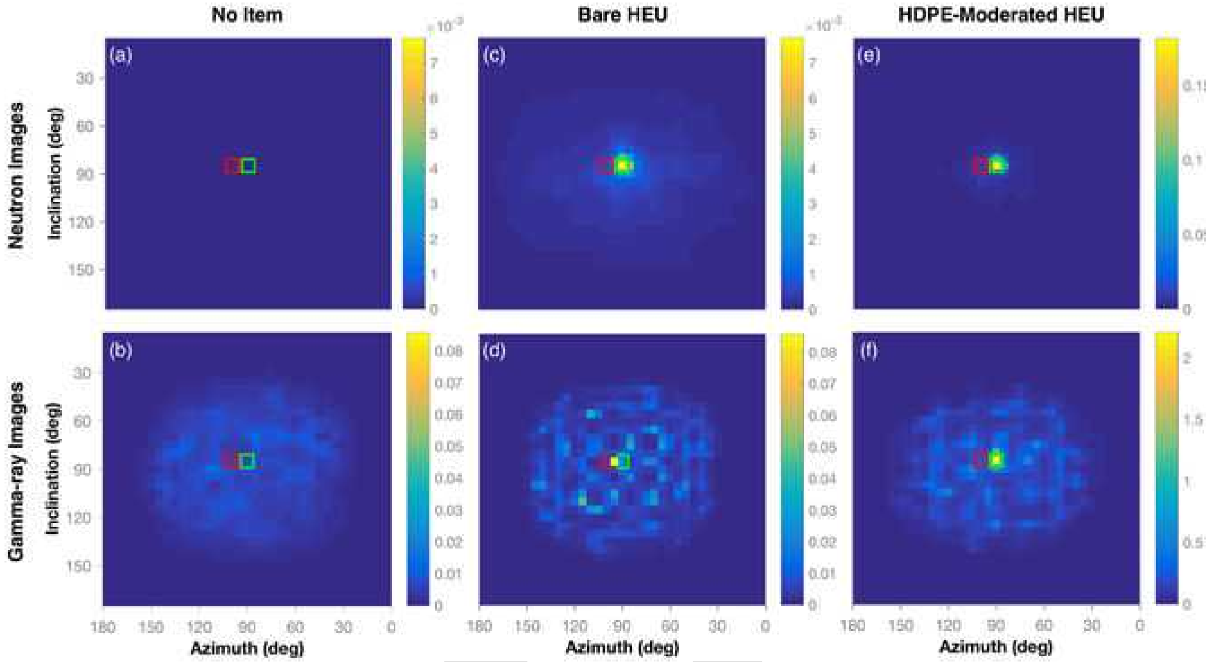

Figure 10. Images from active interrogation experiments

The neutron image reconstructed of the bare HEU shows a hot-spot located within the green box and very small contribution from the red box. The location of the hot-spot provides confidence that the neutrons imaged were from the HEU and not the DT neutron generator. The result shows that the technique is able to correctly image the HEU. To create a well-defined hot-spot from the gamma rays, a lower energy threshold of 2.5 MeV was applied with an upper threshold of 2.8 MeV. This threshold removes a large contribution from the environmental background, and lower energy fission gamma rays, but not the high energy fission gamma rays. The upper threshold removes events that reconstruct poorly due to system resolution effects. The hot-spot is not centered in the green box; it appears in the pixel between the red and green box. To directly compare the gamma-ray image with no item present (Fig. 10(b)) to the image of the bare HEU configuration (Fig. 10(d)), the 2.5-MeV lower and 2.8-MeV upper thresholds were also applied. The comparison shows that the inclusion of bare HEU produces the hot-spot in Fig. 10(d), despite it not occurring in the expected pixel.

DISCUSSION:

PASSIVE WGPU EXPERIMENTS

In this experiment it was demonstrated that the SOE algorithm could be used as a first step towards discriminating and identifying SNM in an environment where other radioactive sources are present. In this case, it was significant to show that the neutron spectra for WGPu and ^{252}Cf had the same shape (Fig. 7(b)) and average energy. Of course further steps would be required to make a robust identification – especially if shielding has changed the spectral shape. Unfolding the isolated spectra would be the another step in identification because it would remove the resolution and efficiency effects found in the reconstructed spectra. This would transform the isolated spectra into a closer representation of the actual emitted spectra.

This experiment also showed that a source completely invisible to gamma-ray detection by the DPI was detected and imaged using the neutron signal, which demonstrates the advantage of dual-particle sensitivity. A system detecting both particle types has a better chance of finding all present sources of SNM in an environment, especially if shielding is present.

Using the gamma-ray signal allowed identification of a difference in the signal produced by the WGPu and the ^{252}Cf. The normalized gamma-ray spectra (Fig. 9(b)) show features that can be used to identify and discriminate WGPu from other gamma-ray sources. Two large peaks are seen in the WGPu at 0.38 MeV and 0.640 MeV which are not prominent in the ^{252}Cf spectrum. There are two notable features seen in the ^{252}Cf spectrum that may make identification more difficult. The first is a shoulder at about 0.48 MeV from gamma-rays created by the (n,α) reaction on ^{10}B, present in the liquid scintillator optical windows, and the second is a small peak at 0.62 MeV from built-up fission products and a contamination from WGPu origins. Due to the age of the source, ^{249}Cf is also present in the sample which emits a 0.388-MeV gamma-ray with an intensity of 66%. Further characterization of the SOE algorithm may provide a method for quantification and subtraction of contamination of origins in the wrong spectrum. We must also seek to understand the effect of gamma-ray production from neutron interactions in our detectors when a large field of slower neutrons is present.

In this experiment, the source localization was consistent with the prior two experiments. In future work we will seek to combine the neutron and gamma-ray cones to generate a combined SOE reconstruction. This may assist with some of the localization discrepancies seen in these experiments. Using smaller pixels may also provide more insight into the accuracy of the localization, however, finer pixels require more iterations for convergence making the problem more computationally expensive.

ACTIVE HEU EXPERIMENTS

The active interrogation experiments provided key insight into the challenges associated with active interrogation. The DT generator was pulsed to provide a means for discriminating the 14.1-MeV neutrons produced by the generator from the neutrons produced by induced fission in the HEU. Recording the start of the generator pulse allowed for a time cut to be implemented on the data ensuring that only neutrons from the HEU were imaged. This method was not explored in detail and leaves room for potential future improvement. While the generator emitted neutrons in all directions, the emission was not uniform [5]. Determining the neutron flux directed at the HEU was estimated and not a straightforward setting on the generator. An error in the flux of up to 25% is possible because only a single setting was certified by the manufacturer for this neutron generator [5]. Future active interrogation experiments may attempt to capture the true neutron emission towards the HEU to better understand the induced fission and detected count rates.

The small error in localization is statistical in nature and not due to a systematic bias. A low signal-to-noise ratio and limited number of correlated gamma rays detected from the HEU likely produced the error. The correlated count rate with the applied energy window with the HEU present was 3.2706 ± 0.0304 and was 3.0905 ± 0.0858 with no item. These correlated count rates provide an estimate that only 638 ± 322 total counts were measured from the HEU in the 59-minute measurement while 10940 ± 304 total counts were from the active background.

ANTICIPATED OUTCOMES AND IMPACTS:

The impacts of this work may be wide ranging if implemented in future imaging efforts to improve verification. At this point imaging techniques are not ubiquitous in the arms-control community. A large reason for this is the complexity of systems required to produce images. Gamma-ray imaging is a more mature technology at this point compared to fast neutron imaging. The lag in neutron capabilities is likely due to the challenges of neutron detection in general. It is very difficult to gain full energy information from neutrons as they are most often detected through elastic scattering. As such, any improvements in image reconstruction methodologies to improve resolution and signal to noise ratio lessen the burden on detector development to improve imaging results.

Experiments demonstrating imaging capabilities using actual SNM also makes a large impact. Researchers have very limited access to large quantities of SNM, which prevents challenges not experienced for common surrogate sources such as ^{252}Cf. For example, low energy gamma-rays from WGPu are emitted at very high intensities which can overload data acquisition systems or cause potential noise in the desired signal.

Exploring imaging as it relates to arms-control presents an opportunity for new research. A multitude of issues arise that would not be present in other non-proliferation applications. For example, authentication and certification of complex multi-detector systems producing rich data streams may be explored. Also, studies concerning image resolution would provide a basis for improving or even limiting resolution. Improvements may be desired to see shapes or fissile material while resolution limits may be useful if only item counting is desired.

SOE ALGORITHM

Modifications to the SOE algorithm may allow for better reconstructed image quality. The underlying Bayesian prior used to create the acceptance probability for origins can be further optimized depending on system parameters or application specific knowledge, such as an expected source distribution [6]. Other efforts to improve SOE are focused on improving reconstruction time through parallelization of the algorithm [7,8]. These techniques have examined handling iterative origin sampling in parallel using graphical processing units. Furthermore, improvements can be made to the implementation of the SOE algorithm to improve spectral isolation if required by the application. As implemented in this work, SOE approximates a uniform efficiency across the image space. Using a simulated system response matrix that calculates spatially-dependent efficiencies can improve localization. Adjusting individual event probabilities based on these efficiencies would likely remove some artifacts primarily seen in the SOE gamma-ray images and improve the appearance of extended sources. The response matrix could also be used to unfold isolated spectra, which would improve the resolution and aid in isotopic identification. This technique was partially demonstrated in [9].

The robust energy information provided by the system and spectral isolation may also provide the necessary information to infer or quantify intervening material present between sources and the DPI. Because SOE preserves the individual properties associated with each event, an opportunity exists to examine time spectra for double-scatter events. This would allow the neutron lifetime to be isolated for multiple sources to determine if the source is multiplying or not. Detection of a correlated neutron event with a gamma ray from the same fission or fission chain would also allow for time-correlated pulse-height analysis to be isolated for multiple sources [10]. Investigating the combination of neutron and gamma-ray data for SOE image reconstruction may also improve results when shielding is present or a low signal-to-background is present.

PASSIVE WGPU EXPERIMENTS

The work with passive detection should be extended to examine other item attributes beyond spectroscopy. The organic liquid scintillators provide excellent timing properties which could be leveraged to examine fission chain properties. If the length of fission chain can be quantified, it may be possible to quantify properties such as item multiplication or fissile mass.

ACTIVE HEU EXPERIMENTS

Several extensions to this work can be made to improve verification capabilities. The resolution of the DPI could be improved to allow for the shape of the item to be evaluated instead of appearing as a point source. Moving the system closer to the interrogated item would increase the signal-to-background ratio for gamma rays, which could provide for their spectral analysis. To detect more induced fission particles, the use of a collimated DT source would allow for continuous interrogation (without pulsing) and all measured counts could be attributed to the HEU without use of a veto. Finally, a characterization of time-dependent neutron count rate, which differ with changing ^{235}U mass, may be performed and tested with items of differing mass and enrichment, which may allow for conclusions to be drawn about the mass of ^{235}U in an item.

CONCLUSION:

The DPI was found to be a successful tool for localizing large quantities of SNM and recording energy information. Paired with the SOE algorithm and spectral isolation capabilities, individual sources can be discriminated from one another based on their energy spectra in a measurement with multiple sources.

PASSIVE WGPU EXPERIMENTS

These experiments provided isolated energy spectra from a single image that made it possible to discriminate a ^{9}Be(α,n) neutron spectrum from a Watt fission neutron spectrum using the SOE algorithm for image reconstruction. The AmBe had an average energy of 3.85 MeV, which was higher than the average energies of the WGPu and ^{252}Cf spectra of 3.23 MeV and 3.20 MeV respectively. Due to the similar shape and average energies of the WGPu and ^{252}Cf neutron spectra, the isolated gamma-ray spectra were needed to discriminate the two sources. The isolated WGPu spectrum showed two prominent peaks at 0.38 MeV and 0.64 MeV which are consistent with decay energies from WGPu. The isolated ^{252}Cf spectrum did not feature these prominent peaks but was consistent with a gamma-ray spectrum from fission.

ACTIVE HEU EXPERIMENTS

These active interrogation experiments demonstrated that the DPI paired with a DT neutron generator can determine the location of an interrogated 13.7-kg HEU item. Results showed that a source-to-system distance of 155 cm and a generator output of approximately 7×10^{7} neutrons per second was sufficient for locating 13.7 kg of HEU in one hour or less depending on the moderation. When the HEU was bare, detection of neutrons produced a high quality image while the gamma-ray image suffered from a low signal-to-background ratio. Despite including an energy threshold to eliminate low energy environmental background, there was still a small error in localization. Moderation with HDPE greatly improved the imaging due to an increase in detected neutrons and gamma-rays. The HDPE increased the item multiplication by reflecting emitted neutron back into the HEU where they induced more fissions reactions.

REFERENCES:

[1] A. Poitrasson-Rivière, M. C. Hamel, J. K. Polack, M. Flaska, S. D. Clarke, and S. A. Pozzi, “Dual-particle imaging system based on simultaneous detection of photon and neutron collision events," Nuclear Instruments and Methods in Physics Research, Section A: Accelerators, Spectrometers, Detectors and Associated Equipment, vol. 760, pp. 40-45, 2014.

[2] A. Poitrasson-Rivière, J. K. Polack, M. C. Hamel, D. D. Klemm, K. Ito, A. T. McSpaden, M. Flaska, S. S. D. Clarke, S. S. A. Pozzi, A. Tomanin, and P. Peerani, “Angular-resolution and material-characterization measurements for a dual-particle imaging system with mixed-

oxide fuel," Nuclear Instruments and Methods in Physics Research, Section A: Accelerators, Spectrometers, Detectors and Associated Equipment, vol. 797, pp. 278-284, 2015.

[3] A. Sitek, "Representation of photon limited data in emission tomography using origin ensembles," Physics in medicine and biology, vol. 53, no. 12, pp. 3201-3216, 2008.

[4] N. Bissantz, B. A. Mair, and A. Munk, "A multi-scale stopping criterion for MLEM reconstructions in PET," 2006 IEEE Nuclear Science Symposium Conference Record, vol. 6, pp. 3376-3379, 2006.

[5] R. Remetti, L. Lepore, and N. Cherubini, "Development and experimental validation of a monte carlo modeling of the neutron emission from a d-t generator," Nuclear Instruments and Methods in Physics Research, Section A: Accelerators, Spectrometers, Detectors and Associated Equipment, vol. 842, pp. 7-13, 2017.

[6] A. Sitek, Statistical Computing in Nuclear Imaging. CRC Press, 2014.

[7] A. Andreyev, A. Sitek, and A. Celler, "Fast image reconstruction for Compton camera using stochastic origin ensemble approach.," Medical physics, vol. 38, no. 1, pp. 429-438, 2011.

[8] F. X. Avila-Soto, A. N. Beri, E. Valenzuela, A. Wudenhe, A. R. Blenkhorn, J. S. Graf, S. Khuvis, M. K. Gobbert, and J. Polf, "Parallelization for Fast Image Reconstruction using the Stochastic Origin Ensemble Method for Proton Beam Therapy," Technical Report HPCF–2015–27, 2015.

[9] M. C. Hamel, J. K. Polack, A. Poitrasson-Rivière, D. D. Klemm, M. Flaska, S. D. Clarke, S. A. Pozzi, A. Tomanin, and P. Peerani, "Time-of-flight neutron spectrum unfolding for mixed-oxide nuclear fuel and plutonium metal using a dual-particle imager," 2014 IEEE Nuclear Science Symposium and Medical Imaging Conference, pp. 1-5, 2014.

[10] M. Monterial, P. Marleau, M. Paff, S. Clarke, and S. Pozzi, "Multiplication and Presence of Shielding Material from Time-Correlated Pulse-Height Measurements of Subcritical Plutonium Assemblies," Nuclear Instruments and Methods in Physics Research Section A: Accelerators, Spectrometers, Detectors and Associated Equipment, vol. 851, pp. 50-56, 2017.